

COVER PAGE

Document downloaded by @DAEL

Thu Nov 26 23:17:33 2026
For personal use

When automatic English translation is provided, only the original document is authentic.
The EAA cannot be held responsible of any translation error

Bibliographical reference

Radially Composite Ultrasonic Transducers of Piezoelectric Ceramic and Metal Circular Rings, Jianzhong Guo, Shuyu Lin, Chenghui Wang and Zhiqiang Fu, Acta Acustica **vol. 98** (Number 4), 2012, pp. 555-566

DOI
https://doi.org/10.3813/AAA.918537

ACTA ACUSTICA UNITED WITH ACUSTICA
Vol. 98 (2012) 555 – 566
DOI 10.3813/AAA.918537

Radially Composite Ultrasonic Transducers of Piezoelectric Ceramic and Metal Circular Rings

Jianzhong Guo, Shuyu Lin, Chenghui Wang, Zhiqiang Fu
Applied Acoustics Institute, Shaanxi Normal University, Xian, Shaanxi, 710062, China. sylin@snnu.edu.cn

Summary
A new type of radially composite ultrasonic transducers in radial vibration is presented and studied. The composite transducer is composed of a radially polarized piezoelectric ceramic ring and a metal ring. The radial vibrations of the radially polarized piezoelectric ring and the metal ring are analyzed and their electro-mechanical equivalent circuits are obtained. Based on the mechanical boundary conditions between the piezoelectric ring and the metal ring, the six-port electro-mechanical equivalent circuit of the radially composite ultrasonic transducer is obtained and the frequency equation is given. The theoretical relationship between the resonance/anti-resonance frequency and the effective electro-mechanical coupling coefficient with the geometrical dimensions of the composite transducer is analyzed. At the same time, the radial vibration of the composite transducer is simulated by using Finite Element Method. The vibrational modal shape and the harmonic response are given numerically. At last, some radially composite ultrasonic transducers are designed and manufactured; their resonance/anti-resonance frequencies are measured. It is shown that the analytical resonance/anti-resonance frequencies are in good agreement with the numerically simulated and experimental results. It is expected that this type of radially composite ultrasonic transducers can be used in large scale ultrasonic liquid processing, such as ultrasonic extraction, ultrasonic sonochemistry and other applications where large radiation surface and ultrasonic power are needed.

PACS no. 43.38.Ar, 43.38.Fx

1. Introduction

The longitudinally composite ultrasonic transducer in longitudinal vibration invented by French scientist Langevin which is also called the longitudinally sandwiched piezoelectric ultrasonic transducer has been widely used in the fields of power ultrasonics and underwater sound [1, 2, 3]. This kind of longitudinally composite ultrasonic transducers is composed of the longitudinally polarized piezoelectric ceramic rings and the end metal masses which are clamped together in the longitudinal direction by some kind of high-strength metal screw bolt. When the longitudinal transducer is excited by an alternating electric signal, sound radiation is produced in the longitudinal direction. The longitudinally composite ultrasonic transducer is a kind of high-intensity transducer; its output power is limited because its radiation surface is limited to less than a quarter of the corresponding longitudinal wavelength. In some ultrasonic applications where large ultrasonic power is needed, the transducer array consisting of a number of longitudinal transducers may be used.

The output power of transducers is determined by the radiation impedance and the vibrational displacement amplitude at the radiation surface. In general cases, the radiation impedance is directly related to the radiation surface area. In order to increase the radiation surface area and therefore the radiation impedance, the ultrasonic vibrating system in coupled vibration of longitudinal and radial vibrations are proposed and studied. Iula studied the Langevin-type transducer with comparable longitudinal and radial dimensions to produce both longitudinal and radial vibrations [4, 5]. Peshkovsky and Dahlem proposed the radially vibrating system, which can give radiation in longitudinal and radial directions [6, 7]. The tubular transducers were also developed to improve the action range of ultrasonic radiation [8, 9]. The cylindrical piezoelectric transducer in radial vibration can be used to meet the requirement of large radiating surface. Compared with the longitudinal composite transducer, the radially composite cylindrical piezoelectric transducer has the advantage of large radiating surface and two-dimensional acoustic radiation. In our previous works, the radially composite cylindrical piezoelectric transducer where the piezoelectric ring is polarized in the thickness direction was analyzed, the electro-mechanical equivalent circuit was derived, and the resonance/anti-resonance frequency equations were given [10, 11, 12].

The cylindrical piezoelectric transducer in radial vibration where the piezoelectric ring is radially polarized is more preferable in producing two-dimensional radial

Received 12 October 2011,
accepted 31 May 2012.

© S. Hirzel Verlag · EAA

sound radiation. Adelman studied the axisymmetric vibration of radially polarized piezoelectric ceramic cylinders and the composite system of the piezoelectric and metal cylinders and disks [13, 14]. In their analysis, the electroelastic equations were established for the piezoelectric ceramic long tubes, the eigenfrequency equations were derived for the resonance and anti-resonance of long tubes and thin disks composed of n radially polarized piezoceramic materials bonded at their cylindrical interfaces. In Reference [15, 16], the radial vibration of the radially polarized piezoelectric ring or tube was studied where the material properties were simplified to be isotropic and the wall thickness of the piezoelectric ring was assumed to much less than the radius and the height. Liu [17] studied the electro-mechanical model for the cylindrical radial composite piezoelectric ceramic transducer where the thin-walled piezoelectric ceramic tube was assumed. In our recent publication [18], the radial vibration of a radially polarized piezoelectric tubular transducer was analyzed where the height is assumed to be much larger than its radial dimension, and therefore a plane strain problem is assumed.

In this paper, the radially composite piezoelectric transducer in radial vibration is further studied. In the following analysis, there is no limitation for the wall thickness of the radially polarized piezoelectric ring. The six-port electromechanical equivalent circuit of the composite transducer is obtained analytically and the frequency equation for the design of the transducer is given. In the following sections, the analytical and numerical methods are used to study the radial vibration of the radially composite piezoelectric transducer, respectively. Experimental results are given and compared with the analytical and numerical results.

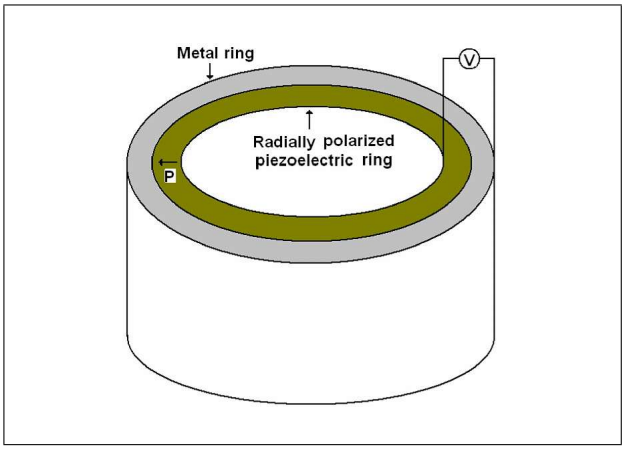


Figure 1. Schematic diagram of a radially composite ultrasonic transducer of the radially polarized piezoelectric ring and the metal ring.

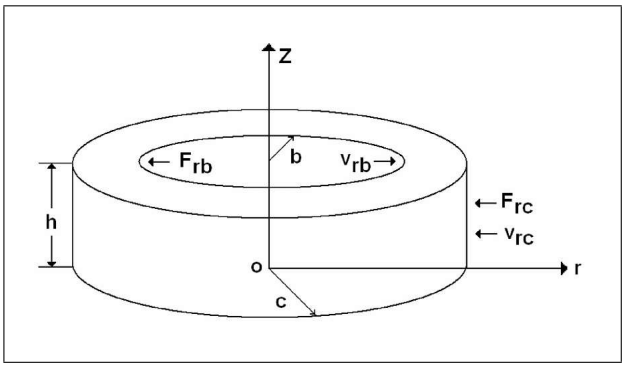


Figure 2. Schematic diagram of a metal thin circular ring in radial vibration.

2. Radial vibration and electro-mechanical equivalent circuit of the radially composite ultrasonic transducer of piezoelectric and metal rings

The radially composite ultrasonic transducer of the radially polarized piezoelectric ring and the metal ring is shown in Figure 1 schematically. In the figure, the piezoelectric ceramic ring is coated with metal electrodes on its inner and outer cylindrical surfaces and is radially polarized; the arrow P represents the polarization direction. The metal ring is outside the piezoelectric ring. The piezoelectric ring and the metal ring are clamped together tightly in the radial direction by the method of heat expansion and cold contraction. When an external exciting electric field is added across the two metal electrodes of the piezoelectric ring, the composite transducer will produce vibration because of the piezoelectric effect. When the height of the transducer is less than its radial dimension, the vibration of the composite transducer can be reduced to the pure radial vibration. In this case, the vibration of the composite transducer can be simplified to the plane stress vibrational problem. It is obvious that the sound radiation of the radially composite cylindrical transducer is two-dimensional. Compared with the longitudinally composite piezoelectric transducer, the radially composite cylindrical transducer has the advantage of large radiation surface and two-dimensional sound radiation.

It should be noted that apart from the condition that the height of the transducer must be much less than the radial dimension, the assumption that the height must be less than the radial wall thickness of the transducer should also be made. When these conditions are fully satisfied, the radial resonance frequencies are much lower than the thickness resonance frequencies of the transducer. In these cases, the coupled vibration between the thickness vibration and the radial vibration in the transducer can be ignored, and the vibration of the composite transducer can be therefore reduced to simple plane radial vibration. More details about the relationship between the resonance frequency and the geometrical dimensions can be found in References [19, 20].

In the following analysis, the radial vibrations of the metal thin ring and the radially polarized piezoelectric ceramic thin ring with arbitrary wall thickness in the composite transducer are analyzed, respectively, their electromechanical equivalent circuits are obtained and the resonance frequency equation is given.

2.1. Four-port electro-mechanical equivalent circuit of a metal thin ring in radial vibration

A metal thin circular ring in radial vibration is shown in Figure 2. Its height, outer and inner radiuses are h, c and b, respectively. In the figure, v_{rc}, v_{rb} and F_{rc}, F_{rb} are radial vibrational velocities and external forces at the outer and inner surfaces. The following equations for a thin metal circular ring in polar co-ordinates can be obtained as [21]

$$\rho\frac{\partial^2\xi_r}{\partial t^2} = \frac{\partial T_r}{\partial r} + \frac{T_r - T_\theta}{r}, \tag{1}$$

$$T_r = \frac{E}{1-\nu^2}\big(S_r + \nu S_\theta\big),$$

$$T_\theta = \frac{E}{1-\nu^2}\big(S_\theta + \nu S_r\big), \tag{2}$$

$$S_r = \frac{\partial\xi_r}{\partial r}, \qquad S_\theta = \frac{\xi_r}{r}, \tag{3}$$

where ξ_r is radial vibrational displacement, T_r and T_θ are radial and tangential stress components, S_r and S_θ are radial and tangential strains. ρ is density, E and ν are Young's modulus and Poisson's ratio. Based on these equations, the wave equation for a metal thin ring in radial vibration can be obtained as

$$\frac{\partial^2\xi_r}{\partial t^2} = V_r^2\left(\frac{\partial^2\xi_r}{\partial r^2} + \frac{1}{r}\frac{\partial\xi_r}{\partial r} - \frac{\xi_r}{r}\right), \tag{4}$$

where $V_r^2 = E/[\rho(1-\nu^2)]$, V_r is sound propagation speed of radial vibration in a metal thin circular ring. The solution to equation (4) is

$$\xi_r = \big[AJ_1(kr) + BY_1(kr)\big]\mathrm{e}^{\mathrm{j}\omega t}, \tag{5}$$

where $k = \omega/V_r$, ω is angular frequency, $J_1(kr)$ and $Y_1(kr)$ are the first and second kind of Bessel functions of order one, A and B are two constants, they can be determined by the boundary conditions of the metal ring. From equation (5), the radial vibrational velocity can be obtained,

$$v_r = \mathrm{j}\omega\big[AJ_1(kr) + BY_1(kr)\big]\mathrm{e}^{\mathrm{j}\omega t}. \tag{6}$$

From Figure 1, when $r = c$, $v_r = -v_{rc}$; when $r = b$, $v_r = v_{rb}$. Therefore, the constants A and B can be obtained as

$$B = \frac{1}{\mathrm{j}\omega}\frac{v_{rc}J_1(kb) + v_{rb}J_1(kc)}{J_1(kc)Y_1(kb) - J_1(kb)Y_1(kc)}\mathrm{e}^{-\mathrm{j}\omega t}, \tag{7}$$

$$A = -\frac{1}{\mathrm{j}\omega}\frac{v_{rc}Y_1(kb) + v_{rb}Y_1(kc)}{J_1(kc)Y_1(kb) - J_1(kb)Y_1(kc)}\mathrm{e}^{-\mathrm{j}\omega t}. \tag{8}$$

Substituting these two expressions into the expression of radial stress T_r in equation (2) yields

$$T_r = \frac{Ek}{1-\nu^2}\Big\{A\Big[J_0(kr) - \frac{(1-\nu)J_1(kr)}{kr}\Big] + B\Big[Y_0(kr) - \frac{(1-\nu)Y_1(kr)}{kr}\Big]\Big\}\mathrm{e}^{\mathrm{j}\omega t}. \tag{9}$$

Using the force boundary conditions of $F_r = T_r\big|_{r=c}\cdot S_{rc} = -F_{rc}$ and $F_r = T_r\big|_{r=b}\cdot S_{rb} = -F_{rb}$, we have

$$F_{rc} = -\frac{ES_{rc}}{1-\nu^2}\frac{k}{\mathrm{j}\omega\big[J_1(kc)Y_1(kb) - J_1(kb)Y_1(kc)\big]} \cdot\Big\{v_{rc}\Big[Y(c)J_1(kb) - J(c)Y_1(kb)\Big] + v_{rb}\Big[Y(c)J_1(kc) - Y_1(kc)J(c)\Big]\Big\}, \tag{10}$$

$$F_{rb} = -\frac{ES_{rb}}{1-\nu^2}\frac{k}{\mathrm{j}\omega\big[J_1(kc)Y_1(kb) - J_1(kb)Y_1(kc)\big]} \cdot\Big\{v_{rc}\Big[Y(b)J_1(kb) - J(b)Y_1(kb)\Big] + v_{rb}\Big[Y(b)J_1(kc) - Y_1(kc)J(b)\Big]\Big\}. \tag{11}$$

Here, $S_{rc} = 2\pi ch$, $S_{rb} = 2\pi bh$, S_{rc} and S_{rb} are outer and inner cylindrical surface areas of a metal ring. In equations (10) and (11), $J(c)$, $J(b)$ and $Y(c)$, $Y(b)$, are four introduced functions, their expressions are

$$J(c) = J_0(kc) - \frac{(1-\nu)J_1(kc)}{kc},$$

$$J(b) = J_0(kb) - \frac{(1-\nu)J_1(kb)}{kb}, \tag{12}$$

$$Y(c) = Y_0(kc) - \frac{(1-\nu)Y_1(kc)}{kc},$$

$$Y(b) = Y_0(kb) - \frac{(1-\nu)Y_1(kb)}{kb}. \tag{13}$$

After some transformations, equations (10) and (11) can be rewritten as

$$\frac{F_{rc}}{\mathrm{j}Z_c} = v_{rc}\Big[\frac{1-\nu}{kc} + \frac{Y_0(kc)J_1(kb) - J_0(kc)Y_1(kb)}{J_1(kc)Y_1(kb) - J_1(kb)Y_1(kc)}\Big] + v_{rb}\Big[\frac{J_1(kc)Y_0(kc) - J_0(kc)Y_1(kc)}{J_1(kc)Y_1(kb) - J_1(kb)Y_1(kc)}\Big], \tag{14}$$

$$\frac{F_{rb}}{\mathrm{j}Z_b} = v_{rc}\Big[\frac{Y_0(kb)J_1(kb) - J_0(kb)Y_1(kb)}{J_1(kc)Y_1(kb) - J_1(kb)Y_1(kc)}\Big] + v_{rb}\Big[\frac{J_1(kc)Y_0(kb) - J_0(kb)Y_1(kc)}{J_1(kc)Y_1(kb) - J_1(kb)Y_1(kc)} - \frac{1-\nu}{kb}\Big], \tag{15}$$

where $Z_c = \rho V_r S_{rc}$, $Z_b = \rho V_r S_{rb}$. Equations (14) and (15) can be further expressed as

$$F_{rb} = \big(Z_{1m} + Z_{3m}\big)v_{rb} + Z_{3m}v_{rc}, \tag{16}$$

$$F_{rc} = \big(Z_{2m} + Z_{3m}\big)v_{rc} + Z_{3m}v_{rb}, \tag{17}$$

Where Z_{1m}, Z_{2m} and Z_{3m} are three mechanical impedances, and their expressions are

$$Z_{1m} = \mathrm{j}\frac{2Z_{rb}}{\pi kb\big[J_1(kc)Y_1(kb) - J_1(kb)Y_1(kc)\big]} \cdot\Big[J_1(kc)Y_0(kb) - J_0(kb)Y_1(kc) - J_1(kb)Y_0(kb) + J_0(kb)Y_1(kb)\Big] \cdot\Big[J_1(kb)Y_0(kb) - J_0(kb)Y_1(kb)\Big]^{-1} - \mathrm{j}\frac{2Z_{rb}(1-\nu)}{\pi(kb)^2\big[J_1(kb)Y_0(kb) - J_0(kb)Y_1(kb)\big]}, \tag{18}$$

$$Z_{2m} = \mathrm{j}\frac{2Z_{rb}}{\pi kb\left[J_1(kc)Y_1(kb) - J_1(kb)Y_1(kc)\right]} \cdot \Big[J_1(kb)Y_0(kc) - J_0(kc)Y_1(kb) - J_1(kc)Y_0(kc) + J_0(kc)Y_1(kc)\Big] \cdot \Big[J_1(kc)Y_0(kc) - J_0(kc)Y_1(kc)\Big]^{-1} + \mathrm{j}\frac{2Z_{rc}(1-\nu)}{\pi(kc)^2\left[J_1(kc)Y_0(kc) - J_0(kc)Y_1(kc)\right]}, \quad (19)$$

$$Z_{3m} = \mathrm{j}\frac{2Z_{rb}}{\pi kb\left[J_1(kc)Y_1(kb) - J_1(kb)Y_1(kc)\right]} = \mathrm{j}\frac{2Z_{rc}}{\pi kc\left[J_1(kc)Y_1(kb) - J_1(kb)Y_1(kc)\right]}. \quad (20)$$

From equations (16) and (17), the four-port electro-mechanical equivalent circuit of a metal thin circular ring in radial vibration can be obtained as shown in Figure 3.

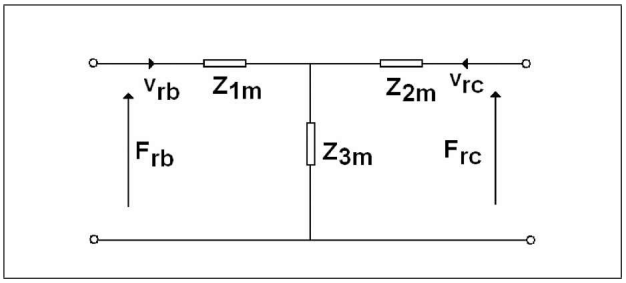


Figure 3. Four-port electro-mechanical equivalent circuit of a metal thin circular ring in radial vibration.

2.2. Six-port electro-mechanical equivalent circuit of a radially polarized piezoelectric thin ring in radial vibration

Figure 4 illustrates a piezoelectric ceramic ring with radial polarization. The electrodes are on the inner and outer cylindrical surfaces. The electric polarization (P) and the external exciting electric field (E) are in the radial direction. The height, the inner and the outer radius of the ring are L, a, b respectively. In the case of a plane stress problem, it is assumed that the height should be less than its outer radius, i.e. $L \ll b$. In this case, the polarization direction, the exciting electric field direction and the vibrational displacement direction are all in the radial direction. For polar coordinates as shown in Figure 4, with the polarization direction being in the radial direction, the coordinate directions r, θ, z will be designated as 3, 1 and 2, respectively.

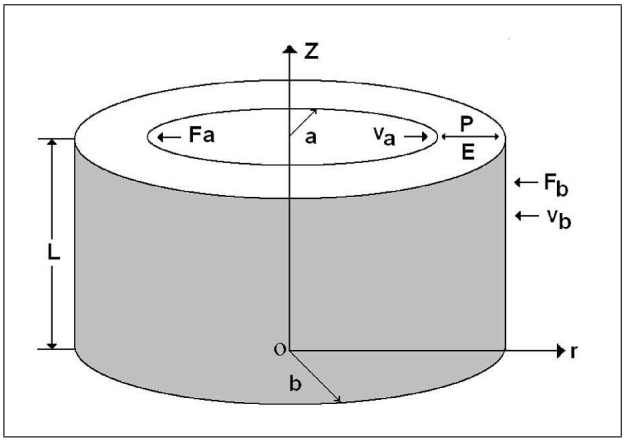


Figure 4. A radially polarized piezoelectric ceramic thin circular ring with arbitrary wall thickness.

2.2.1. Exact analytical theory for the piezoelectric ceramic thin ring with arbitrary wall thickness

The piezoelectric constitutive equations in polar coordinates can be expressed as [22]

$$T_\theta = c_{11}^E S_\theta + c_{12}^E S_z + c_{13}^E S_r - e_{31}E_r, \quad (21)$$

$$T_z = c_{11}^E S_\theta + c_{11}^E S_z + c_{13}^E S_r - e_{31}E_r, \quad (22)$$

$$T_r = c_{13}^E S_\theta + c_{13}^E S_z + c_{33}^E S_r - e_{33}E_r, \quad (23)$$

$$D_r = c_{31}^E S_\theta + c_{31}^E S_z + c_{33}^E S_r - \varepsilon_{33}^S E_r, \quad (24)$$

where $E_r = E_r(r,t)$ is the radial exciting electric field, $D_r = D_r(r,t)$ is electric displacement. c_{ij}^E, e_{ij}, ε_{ij}^S are the elastic constants, piezoelectric constants and the dielectric constants, respectively. In the case of plane stress, we have $T_z = 0$. From equation (22), we have

$$S_z = \frac{c_{12}^E S_\theta + c_{13}^E S_r - e_{31}E_r}{c_{11}^E}. \quad (25)$$

Substituting equation (25) into (21), (23) and (24) yields,

$$T_\theta = \Big(c_{11}^E - \frac{c_{12}^E c_{12}^E}{c_{11}^E}\Big)S_\theta + \Big(c_{13}^E - \frac{c_{12}^E c_{13}^E}{c_{11}^E}\Big)S_r - \Big(e_{31} - \frac{e_{31}c_{12}^E}{c_{11}^E}\Big)E_r, \quad (26)$$

$$T_r = \Big(c_{13}^E - \frac{c_{12}^E c_{13}^E}{c_{11}^E}\Big)S_\theta + \Big(c_{33}^E - \frac{c_{13}^E c_{13}^E}{c_{11}^E}\Big)S_r - \Big(e_{33} - \frac{e_{31}c_{13}^E}{c_{11}^E}\Big)E_r, \quad (27)$$

$$D_r = \Big(e_{31} - \frac{e_{31}c_{12}^E}{c_{11}^E}\Big)S_\theta + \Big(e_{33} - \frac{e_{31}c_{13}^E}{c_{11}^E}\Big)S_r + \Big(\varepsilon_{33}^S + \frac{e_{31}e_{31}}{c_{11}^E}\Big)E_r. \quad (28)$$

Since the piezoelectric ceramic material is assumed to be an ideal insulating medium, there is no free charge in it. Therefore, the static charge equation can be expressed as

$$\frac{1}{r}\frac{\partial(rD_r)}{\partial r} = 0. \quad (29)$$

The solution to equation (29) is

$$D_r = \frac{A_3}{r}\mathrm{e}^{\mathrm{j}\omega t}, \quad (30)$$

where A_3 is a constant, it can be determined by the electric boundary conditions.

2.2.2. Mechanical vibrational characteristics of the piezoelectric ceramic ring

In the case of harmonic vibration, the radial displacement and the electric field can be expressed as

$$\xi_r = \xi_{r0} e^{j\omega t}, \tag{31}$$

$$E_r = E_{r0} e^{j\omega t}, \tag{32}$$

where ξ_{r0} and E_{r0} are amplitudes of the radial displacement and the electric field strength. Substituting equation (30) into (28) yields

$$E_{r0} = b_3 S_\theta + b_5 S_r + \frac{c_{11}^E}{\varepsilon_{33}^S c_{11}^E + e_{31} e_{31}} \frac{A_3}{r}, \tag{33}$$

where $b_3 = (e_{31} c_{12}^E - e_{31} c_{11}^E)/(\varepsilon_{33}^S c_{11}^E + e_{31} e_{31})$, $b_5 = (e_{31} c_{13}^E - e_{33} c_{11}^E)/(\varepsilon_{33}^S c_{11}^E + e_{31} e_{31})$. Substituting equation (33) into (26) and (27) yields

$$T_\theta = b_1 S_\theta + b_2 S_r + b_3 \frac{A_3}{r}, \tag{34}$$

$$T_r = b_2 S_\theta + b_4 S_r + b_5 \frac{A_3}{r}, \tag{35}$$

where

$$b_1 = \frac{\varepsilon_{33}^S c_{11}^E c_{11}^E - \varepsilon_{33}^S c_{12}^E c_{12}^E + 2 e_{31} e_{31} c_{11}^E - 2 e_{31} e_{31} c_{12}^E}{\varepsilon_{33}^S c_{11}^E + e_{31} e_{31}}, \tag{36}$$

$$b_2 = \frac{\varepsilon_{33}^S c_{11}^E c_{13}^E - \varepsilon_{33}^S c_{12}^E c_{13}^E + e_{31} e_{33} c_{11}^E - e_{31} e_{33} c_{12}^E}{\varepsilon_{33}^S c_{11}^E + e_{31} e_{31}}, \tag{37}$$

$$b_4 = \frac{\varepsilon_{33}^S c_{11}^E c_{33}^E - \varepsilon_{33}^S c_{13}^E c_{13}^E + e_{31} e_{31} c_{33}^E - e_{33} e_{33} c_{11}^E}{\varepsilon_{33}^S c_{11}^E + e_{31} e_{31}}. \tag{38}$$

Substituting equations (30) and (34), (35) into the wave equation (1) yields the motion equation

$$\rho \frac{\partial^2 \xi_r}{\partial t^2} = b_4 \left(\frac{\partial^2 \xi_r}{\partial r^2} + \frac{1}{r} \frac{\partial \xi_r}{\partial r} - \nu^2 \frac{\xi_r}{r^2} - \frac{b_3}{b_4} \frac{A_3}{r^2} \right). \tag{39}$$

In equation (39), $\nu^2 = b_1/b_4$. Substituting $\xi_r = \xi_{r0} e^{j\omega t}$ into (39) yields

$$\frac{d^2 \xi_{r0}}{dr^2} + \frac{1}{r} \frac{\partial \xi_{r0}}{\partial r} + \left(k^2 - \nu^2/r^2\right) \xi_{r0} - b_3' \frac{A_3}{r^2} = 0, \tag{40}$$

where $b_3' = b_3/b_4$, $k = \omega/V_3$, $V_3^2 = b_4/\rho$, k and V_3 are wave number and sound speed of radial vibration in a thin piezoelectric ceramic ring polarized in the radial direction. Equation (40) is the generalized Bessel differential equation, or the Lommel differential equation, its solution can be expressed as

$$\xi_{r0} = A_1 J_\nu(kr) + A_2 Y_\nu(kr) + b_3' A_3 s_{-1,\nu}(kr), \tag{41}$$

where $J_\nu(kr)$ and $Y_\nu(kr)$ are Bessel functions of type one and two. $s_{u,\nu}(kr)$ is Lommel function of type one. A_1 and A_2 are two constants. From equation (41), the radial vibrational velocity for the ring is

$$v_{r0} = j\omega \left[A_1 J_\nu(kr) + A_2 Y_\nu(kr) + b_3' A_3 s_{-1,\nu}(kr) \right]. \tag{42}$$

2.2.3. Electrical characteristics of a radially polarized piezoelectric ceramic thin circular ring

From Figure 4, the velocity boundary conditions for the ring can be expressed as

$$v_{r0}\big|_{r=a} = v_a, \qquad v_{r0}\big|_{r=b} = v_b. \tag{43}$$

Substituting equation (42) into (43) yields

$$A_1 J_\nu(ka) + A_2 Y_\nu(ka) + b_3' A_3 s_{-1,\nu}(ka) = \frac{v_a}{j\omega}, \tag{44a}$$

$$A_1 J_\nu(kb) + A_2 Y_\nu(kb) + b_3' A_3 s_{-1,\nu}(kb) = -\frac{v_b}{j\omega}. \tag{44b}$$

From equation (44), the constants and can be obtained,

$$A_1 = -\frac{j Y_\nu(kb)}{\tau_1 \omega} v_a - \frac{j Y_\nu(ka)}{\tau_2 \omega} v_b + \frac{\tau_2}{\tau_1} A_3, \tag{45a}$$

$$A_2 = \frac{j J_\nu(kb)}{\tau_1 \omega} v_a + \frac{j J_\nu(ka)}{\tau_2 \omega} v_b + \frac{\tau_3}{\tau_1} A_3, \tag{45b}$$

where

$$\tau_1 = J_\nu(ka) Y_\nu(kb) - J_\nu(kb) Y_\nu(ka),$$
$$\tau_2 = b_3' Y_\nu(ka) s_{-1,\nu}(kb) - b_3' Y_\nu(kb) s_{-1,\nu}(ka),$$
$$\tau_3 = b_3' J_\nu(kb) s_{-1,\nu}(ka) - b_3' J_\nu(ka) s_{-1,\nu}(kb).$$

The voltage across the inner and outer electrodes of the piezoelectric ring can be expressed as

$$V_{r0} = -\int_a^b E_{r0}\, dr. \tag{46}$$

Substituting equation (33) into (46), we have

$$\begin{aligned} V_{r0} = {} & -A_1 \left[\int_a^b \frac{b_3 J_\nu(kr)}{r} dr + b_5 J_\nu(kr) \Big|_a^b \right] \\ & - A_2 \left[\int_a^b \frac{b_3 Y_\nu(kr)}{r} dr + b_5 Y_\nu(kr) \Big|_a^b \right] \\ & - A_3 \left[\int_a^b \frac{b_3' b_3 s_{-1,\nu}(kr)}{r} dr + b_3' b_5 s_{-1,\nu}(kr) \Big|_a^b \right. \\ & \left. + \frac{c_{11}(\ln b - \ln a)}{\varepsilon_{33}^S c_{11}^E + e_{31} e_{31}} \right]. \end{aligned} \tag{47}$$

After some complex integration, equation (47) can be expressed as

$$V_{r0} = -\frac{jka\chi_a}{\omega} v_a - \frac{jkb\chi_a}{\omega} v_b - \frac{A_3}{\chi}. \tag{48}$$

In the derivation of equation (48), the following function relations are used:

$$\int \frac{J_\nu(kr)}{r} dr = kr(\nu - 2) J_\nu(kr) s_{-2,\nu-1}(kr) - kr J_{\nu-1}(kr) s_{-1,\nu}(kr), \tag{49}$$

$$\int \frac{Y_\nu(kr)}{r} dr = kr(\nu - 2) Y_\nu(kr) s_{-2,\nu-1}(kr) - kr Y_{\nu-1}(kr) s_{-1,\nu}(kr), \tag{50}$$

$$\int \frac{s_{-1,\nu}(kr)}{r} dr = \int \frac{s_{1,\nu}(kr) - 1}{\nu^2 r} dr = -\frac{\ln(x)}{\nu^2} + \frac{(kr)^2 {}_2F_3\left([1,1],[2,2+\nu/2,2-\nu/2],-(kr)^2/4\right)}{2\nu^2(4-\nu^2)}, \tag{51}$$

where ${}_mF_n([\alpha_1 \dots \alpha_m], [\rho_1 \dots \rho_n], x)$, is the hypergeometric function. In equation (48), $\chi = \tau_1/\Delta$,

$$\chi_a = b_3\Big\{(\nu-2)s_{-2,\nu-1}(ka) - \frac{\big[J_{\nu-1}(ka)Y_\nu(kb) - J_\nu(kb)Y_{\nu-1}(ka)\big]s_{-1,\nu}(ka)}{\tau_1} - \frac{2s_{-1,\nu}(kb)}{\pi ka\tau_1}\Big\} + \frac{b_5}{ka},$$

$$\chi_b = b_3\Big\{(\nu-2)s_{-2,\nu-1}(kb) + \frac{\big[J_{\nu-1}(kb)Y_\nu(ka) - J_\nu(ka)Y_{\nu-1}(kb)\big]s_{-1,\nu}(kb)}{\tau_1} - \frac{2s_{-1,\nu}(ka)}{\pi kb\tau_1}\Big\} + \frac{b_5}{kb},$$

where

$$\begin{aligned}
\Delta = \tau_1\Big\{ & \frac{b_3 b_3'(H_b - H_a)}{2\nu^2(4-\nu^2)} + b_5 b_3'\big[s_{-1,\nu}(kb) - s_{-1,\nu}(ka)\big] \\
& + \left(\frac{c_{11}}{\varepsilon_{33}c_{11} + e_{31}e_{31}} - \frac{b_3 b_3'}{\nu^2}\right)\big(\ln b - \ln a\big)\Big\} \\
& + \tau_2\big\{b_3\big[(\nu-2)(J1_b - J1_a) + J2_a - J2_b\big] \\
& + b_5\big[J_\nu(kb) - J_\nu(ka)\big]\big\} \\
& + \tau_2\big\{b_3\big[(\nu-2)(Y1_b - Y1_a) + Y2_a - Y2_b\big] \\
& + b_5\big[Y_\nu(kb) - Y_\nu(ka)\big]\big\}, \\
J1_\gamma = {} & kr\,J_\nu(kr)s_{-2,\nu-1}(kr), \\
J2_\gamma = {} & kr\,J_{\nu-1}(k)s_{-1,\nu}(kr), \\
Y1_\gamma = {} & kr\,Y_\nu(kr)s_{-2,\nu-1}(kr), \\
Y2_\gamma = {} & kr\,Y_{\nu-1}(kr)s_{-1,\nu}(kr), \\
H(r) = {} & (kr)^2{}_2F_3\big([1,1],[2,2+\nu/2,2-\nu/2], \\
& -(kr)^2/4\big).
\end{aligned}$$

From equation (48), the constant A_3 can be obtained as

$$A_3 = -\frac{\mathrm{j}ka\chi_a\chi}{\omega}v_a - \frac{\mathrm{j}kb\chi_b\chi}{\omega}v_b - \chi V_{r0}. \tag{52}$$

It is obvious that A_3 is independent of $\boldsymbol{r}$.

2.2.4. Six-port electro-mechanical equivalent circuit of a radially polarized piezoelectric ceramic thin circular ring with arbitrary wall thickness

Substituting equations (3) and (41) into (35) yields

$$\begin{aligned}
T_r = {} & A_1\left[\frac{b_2 J_\nu(kr)}{r} + b_4 J_\nu'(kr)\right] \\
& + A_2\left[\frac{b_2 Y_\nu(kr)}{r} + b_4 Y_\nu'(kr)\right] \\
& + A_3\Big\{b_3'\Big[\frac{b_2 s_{-1,\nu}(kr)}{r} \\
& + b_4 s_{-1,\nu}'(kr)\Big] + \frac{b_5}{r}\Big\}.
\end{aligned} \tag{53}$$

Using the stress boundary conditions of $T_a = T_r|_{r=a}$ and $T_b = T_r|_{r=b}$, substituting equations (45) and (52) into (53), the stress boundary conditions can be rewritten as

$$\begin{aligned}
T_a = {} & \Big\{\frac{\mathrm{j}(b_4\nu - b_2)}{\omega a} - \frac{\mathrm{j}\chi k^2 a\chi_a^2}{\omega} \\
& + \frac{\mathrm{j}kb_4\big[J_\nu(kb)Y_{\nu-1}(ka) - J_{\nu-1}(ka)Y_\nu(kb)\big]}{\omega\tau_1}\Big\}v_a \\
& + \Big(-\frac{\mathrm{j}\chi k^2 b\chi_a\chi_b}{\omega} + \frac{\mathrm{j}2b_4}{\pi\omega a\tau_1}\Big)v_b - k\chi\chi_a V_{r0},
\end{aligned} \tag{54a}$$

$$\begin{aligned}
T_b = {} & \Big(-\frac{\mathrm{j}\chi k^2 a\chi_a\chi_b}{\omega} + \frac{\mathrm{j}2b_4}{\pi\omega b\tau_1}\Big)v_a \\
& + \Big\{\frac{\mathrm{j}(b_2 - b_4\nu)}{\omega b} - \frac{\mathrm{j}\chi k^2 b\chi_b^2}{\omega} \\
& + \frac{\mathrm{j}kb_4\big[J_\nu(ka)Y_{\nu-1}(kb) - J_{\nu-1}(kb)Y_\nu(ka)\big]}{\omega\tau_1}\Big\}v_b \\
& - k\chi\chi_b V_{r0}.
\end{aligned} \tag{54b}$$

In the above derivations, the following expressions are used,

$$J_\nu'(x) = -\frac{\nu}{x}J_\nu(x) + J_{\nu-1}(x), \tag{55}$$

$$Y_\nu'(x) = -\frac{\nu}{x}Y_\nu(x) + Y_{\nu-1}(x), \tag{56}$$

$$s_{u,\nu}'(x) = -\frac{\nu}{x}s_{u,\nu}(x) + \big(u+\nu-1\big)s_{u-1,\nu-1}(x). \tag{57}$$

In the above equations, the superscript represents the derivative to the variable x. From Figure 4, we have the radial force boundary conditions of $F_a = F_r|_{r=a} = -T_a S_a$ and $F_b = F_r|_{r=b} = -T_b S_b$. Here, $S_a = 2\pi aL$, $S_b = 2\pi bL$, which are the cylindrical surface areas. Combining equation (54) and the force boundary conditions, the following equations can be obtained,

$$\begin{aligned}
F_a = {} & \Big\{\frac{\mathrm{j}S_a(b_2 - b_4\nu)}{\omega a} + \frac{\mathrm{j}S_a\chi k^2 a\chi_a^2}{\omega} \\
& - \frac{\mathrm{j}S_a kb_4\big[J_\nu(kb)Y_{\nu-1}(ka) - J_{\nu-1}(ka)Y_\nu(kb)\big]}{\omega\tau_1}\Big\}v_a \\
& + \Big(\frac{\mathrm{j}S_a\chi k^2 b\chi_a\chi_b}{\omega} - \frac{\mathrm{j}2S_a b_4}{\pi\omega a\tau_1}\Big)v_b + kS_a\chi\chi_a V_{r0},
\end{aligned} \tag{58a}$$

$$\begin{aligned}
F_b = {} & \Big(\frac{\mathrm{j}S_b\chi k^2 a\chi_a\chi_b}{\omega} - \frac{\mathrm{j}2S_b b_4}{\pi\omega b\tau_1}\Big)v_a \\
& + \Big\{\frac{\mathrm{j}S_b(b_4\nu - b_2)}{\omega b} + \frac{\mathrm{j}S_b\chi k^2 b\chi_b^2}{\omega} \\
& - \frac{\mathrm{j}S_b kb_4\big[J_\nu(ka)Y_{\nu-1}(kb) - J_{\nu-1}(kb)Y_\nu(ka)\big]}{\omega\tau_1}\Big\}v_b \\
& + kS_b\chi\chi_b V_{r0}.
\end{aligned} \tag{58b}$$

Multiplying equations (58a) and (58b) by $b\chi_b$ and $a\chi_a$ yields

$$\begin{aligned}
F_a' = {} & \Big\{-\frac{n^2}{\mathrm{j}\omega C_0} \\
& - Z_a\frac{\mathrm{j}b^2\chi_b^2\big[J_\nu(kb)Y_{\nu-1}(ka) - J_{\nu-1}(ka)Y_\nu(kb)\big]}{\tau_1} \\
& + \frac{\mathrm{j}2\pi Lb^2\chi_b^2(b_2 - b_4\nu)}{\omega}\Big\}v_a' \\
& + \Big(-\frac{n^2}{\mathrm{j}\omega C_0} - Z_a\frac{\mathrm{j}b\chi_a\chi_b}{\pi k\tau_1}\Big)v_b' + nV_{r0},
\end{aligned} \tag{59a}$$

$$F_b' = \Big(-\frac{n^2}{\mathrm{j}\omega C_0} - Z_b \frac{\mathrm{j}a\chi_a\chi_b}{\pi k \tau_1} \Big) v_a' + \Big\{ -\frac{n^2}{\mathrm{j}\omega C_0} - Z_b \frac{\mathrm{j}a^2\chi_a^2 \big[J_\nu(ka)Y_{\nu-1}(kb) - J_{\nu-1}(kb)Y_\nu(ka) \big]}{\tau_1} + \frac{\mathrm{j}2\pi L a^2 \chi_a^2 (b_4\nu - b_2)}{\omega} \Big\} v_b' + nV_{r0}, \quad (59b)$$

where $Z_a = kb_4S_a/\omega = \rho V_3 S_a$, $Z_b = kb_4S_b/\omega = \rho V_3 S_b$, $F_a' = F_a n_1$, $F_b' = F_b n_2$, $v_a' = v_a/n_1$, $v_b' = v_b/n_2$, $n_1 = b\chi_b$, $n_2 = a\chi_a$, $n = 2\pi L\chi kab\chi_a\chi_b$, $C_0 = 2\pi L\chi$, n is electro-mechanical conversion coefficient, C_0 is the clamped capacitance. The current into the piezoelectric ceramic ring can be obtained according to

$$I_r = -\frac{\mathrm{d}Q}{\mathrm{d}t} = -\mathrm{j}\omega \int_{-L/2}^{L/2} \frac{A_3}{b} b\,\mathrm{d}\theta\,\mathrm{d}z = -\mathrm{j}\omega 2\pi L A_3. \quad (60)$$

Substituting equations (52) into equation (60) yields

$$I_r = -n\big(v_a' + v_b'\big) + \mathrm{j}\omega C_0 V_{r0}. \quad (61)$$

Based on equations (59a), (59b) and (61), the six-port electro-mechanical equivalent circuit for a radially polarized piezoelectric ceramic ring with arbitrary wall thickness can be obtained as shown in Figure 5. In the figure, the expressions for the series and parallel impedances are as

$$Z_1 = -Z_a \frac{\mathrm{j}b^2\chi_b^2 \big[J_\nu(kb)Y_{\nu-1}(ka) - J_{\nu-1}(ka)Y_\nu(kb) \big]}{\tau_1} + \frac{\mathrm{j}2\pi L b^2 \chi_b^2 (b_2 - b_4\nu)}{\omega} + Z_a \frac{\mathrm{j}b\chi_a\chi_b}{\pi k\tau_1}, \quad (62)$$

$$Z_2 = -Z_b \frac{\mathrm{j}a^2\chi_a^2 \big[J_\nu(ka)Y_{\nu-1}(kb) - J_{\nu-1}(kb)Y_\nu(ka) \big]}{\tau_1} + \frac{\mathrm{j}2\pi L a^2 \chi_a^2 (b_4\nu - b_2)}{\omega} + Z_b \frac{\mathrm{j}a\chi_a\chi_b}{\pi k\tau_1}, \quad (63)$$

$$Z_3 = -Z_a \frac{\mathrm{j}b\chi_a\chi_b}{\pi k\tau_1} = -Z_b \frac{\mathrm{j}a\chi_a\chi_b}{\pi k\tau_1}. \quad (64)$$

In Figure 5, the four mechanical terminals m and m', n and n' represent the inner and outer cylindrical surfaces. From Figure 5, it can be seen that the electro-mechanical equivalent circuit for the radial vibration of a radially polarized piezoelectric ring is not symmetrical on the inner and the outer surfaces. It is more complicated and different from the traditional electro-mechanical equivalent circuits for the piezoelectric ring with different polarization and vibrational modes, such as the thickness vibration and radial vibration of a piezoelectric ceramic ring with thickness polarization [12, 23, 24].

2.3. Six-port electro-mechanical equivalent circuit of the radially composite cylindrical ultrasonic transducer

In the above two sections, the equivalent circuits for the radially polarized piezoelectric thin ring and the metal ring have been obtained. From Figure 1, at the radial cylindrical boundary of the piezoelectric and metal rings in the composite transducer, the radial force and velocity are continuous. Therefore, the six-port electro-mechanical equivalent circuit for a radially composite cylindrical ultrasonic transducer of the radially polarized piezoelectric ring and the metal ring can be obtained as shown in Figure 6.

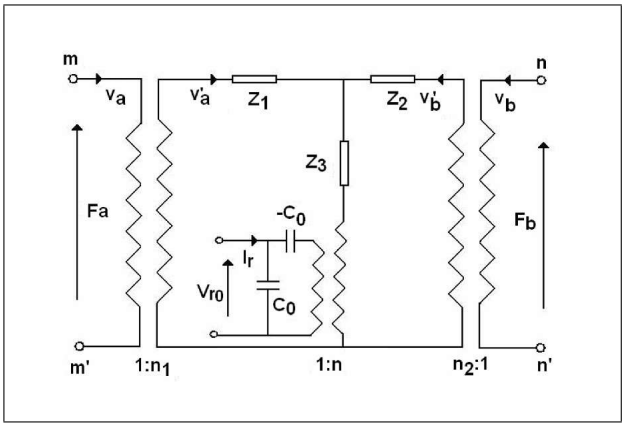


Figure 5. Six-port electro-mechanical equivalent circuit for a radially polarized piezoelectric ceramic thin ring with arbitrary wall thickness.

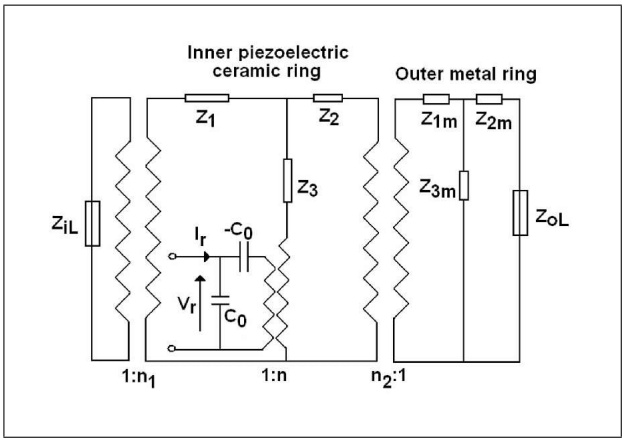


Figure 6. Six-port electro-mechanical equivalent circuit of the radially composite cylindrical ultrasonic transducer.

In the figure, Z_{iL} and Z_{oL} are load mechanical impedances of the transducer at its inner and outer surfaces. In general cases, the inner surface of the transducer is air-backed and therefore Z_{iL} can be regarded as zero. The outer surface of the metal tube is contacted with load medium which determines the load impedance Z_{oL}. The load impedance Z_{oL} is dependable on the working frequency, the geometrical dimension of the transducer, and the load medium. Therefore, its analytical expression is difficult to find. When the load impedance is considered, the input mechanical impedance of the outer metal ring, which can also be regarded as the load mechanical impedance of the inner piezoelectric ring, can be expressed as,

$$Z_{im} = Z_{1m} + \frac{(Z_{2m} + Z_{oL})Z_{3m}}{Z_{2m} + Z_{oL} + Z_{3m}}. \quad (65)$$

From Figure 6, the mechanical impedance of the piezoelectric ring can be obtained,

$$Z_m = Z_3 + \frac{Z_1(Z_2 + n_2^2 Z_{im})}{Z_1 + Z_2 + n_2^2 Z_{im}}. \quad (66)$$

Based on the above equations, the input electric impedance of the composite transducer can be expressed as the form

$$Z_e = \frac{V_r}{I_r} = \frac{n^2 - j\omega C_0 Z_m}{\omega^2 C_0^2 Z_m}. \quad (67)$$

From equation (67), the resonance frequency equation of the composite transducer can be obtained by letting Z_e be zero,

$$n^2 - j\omega C_0 Z_m = 0, \quad (68)$$

and the anti-resonance frequency equation is obtained by letting the Z_e be infinity,

$$\omega^2 C_0^2 Z_m = 0. \quad (69)$$

From the above analysis, it is obvious that the resonance/anti-resonance frequency equations (68) and (69) are complicated transcendental equations. It can be seen that the resonance/anti-resonance frequency of the composite transducer depend on the material property, the geometrical dimensions, the load impedance and the radial vibrational modes. In general cases, when the material and the geometrical dimensions are given, the resonance/anti-resonance frequency can be obtained.

3. Theoretical relationship between the resonance/anti-resonance frequency and the effective electro-mechanical coupling coefficient with the geometrical dimensions of the composite transducer

In this section, the resonance/anti-resonance frequency equations (68) and (69) are solved numerically by using mathematical software (Maple 13 Program). In the calculation, the material for the outer metal ring is stainless steel, its standard material parameters are as follows:

$\rho = 7800\,\mathrm{kg/m^3}$, $E = 2.09 \cdot 10^{11}\,\mathrm{N/m^2}$, $\nu = 2.8$.

The material for the radially polarized piezoelectric ring is PZT-4, its standard material parameters are:

$\rho_0 = 7500\,\mathrm{kg/m^3}$, $c_{11}^E = 13.9 \cdot 10^{10}\,\mathrm{N/m^2}$,
$c_{12}^E = 7.78 \cdot 10^{10}\,\mathrm{N/m^2}$, $c_{13}^E = 7.43 \cdot 10^{10}\,\mathrm{N/m^2}$,
$c_{33}^E = 11.5 \cdot 10^{10}\,\mathrm{N/m^2}$, $e_{31} = -5.2\,\mathrm{Nm/V}$,
$e_{33} = 15.1\,\mathrm{Nm/V}$, $\varepsilon_{33}^S = 5.62 \cdot 10^{-9}\,\mathrm{C/m}$.

Figure 7 is the theoretically simulated relationship between the first radial resonance/anti-resonance frequency and the geometrical dimensions of the transducer and Figure 8 is the theoretically simulated relationship between the second radial resonance/anti-resonance frequency and the geometrical dimensions of the transducer. In the figures, $\tau = (b - a)/(c - a)$, it is defined as the ratio of the thickness of the piezoelectric ceramic ring over that of the composite transducer. It is obvious that when $b = a$, $\tau = 0$, the transducer becomes a metal ring; when $b = c$, $\tau = 1$ the transducer becomes a piezoelectric ring. In the simulation, the inner radius of the ceramic ring and the outer radius of the metal ring are kept constants, $a = 0.01\,\mathrm{m}$, $c = 0.03\,\mathrm{m}$ and $L = 0.005\,\mathrm{m}$.

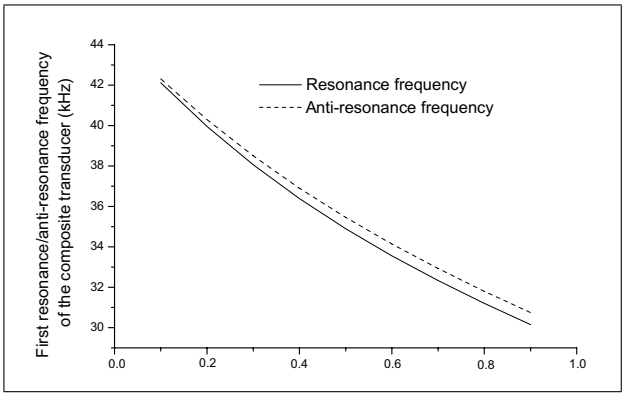


Figure 7. Theoretical relationship between the resonance/anti-resonance frequencies and the geometrical dimensions of the composite transducer in the first radial vibration.

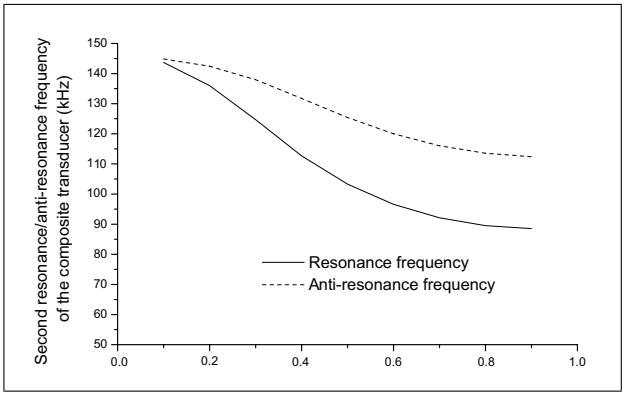


Figure 8. Theoretical relationship between the resonance/anti-resonance frequencies and the geometrical dimensions of the composite transducer in the second radial vibration.

From the simulated results, it can be seen that when the thickness ratio is increased, which means that the thickness of the piezoelectric ring is increased; the resonance and the anti-resonance frequencies are decreased. This means that the resonance and anti-resonance frequencies of a piezoelectric ring are smaller than those of a metal ring with the same geometrical dimensions. The reason for this phenomenon may be that the stiffness of metal material is larger than that of piezoelectric material.

For piezoelectric transducers, the electro-mechanical coupling coefficient is an important parameter. It can be described by

$$K_{\mathrm{eff}} = \left[1 - \left(\frac{f_r}{f_a}\right)^2\right], \quad (70)$$

where f_r and f_a are the resonance and the anti-resonance frequencies. Based on equation (70), the theoretical re-

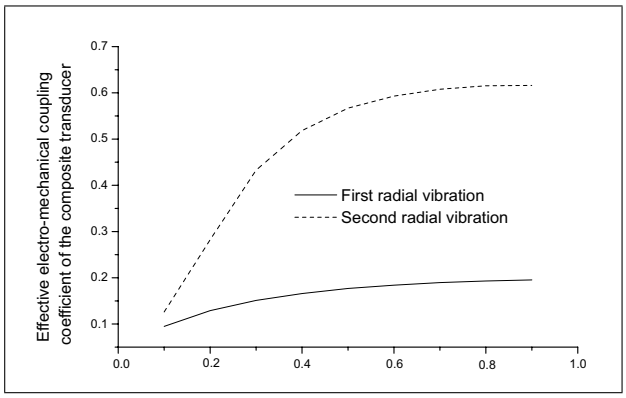


Figure 9. Theoretical relationship between the effective electro-mechanical coupling coefficient and the geometrical dimensions of the composite transducer in the first and the second radial vibration.

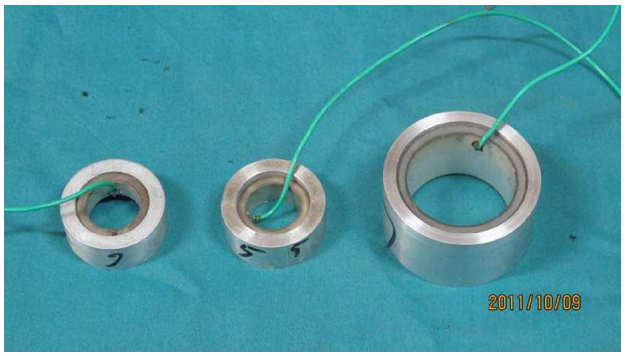


Figure 10. Photograph of the manufactured composite ultrasonic transducers.

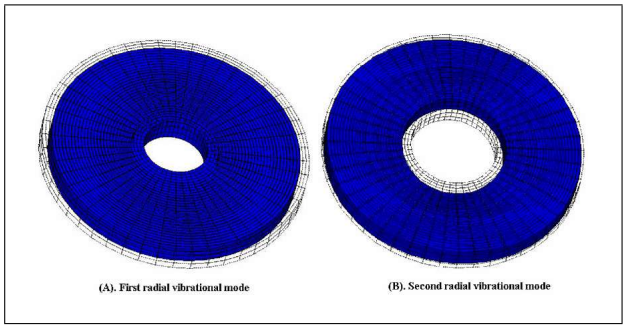


Figure 11. Numerically simulated vibrational modal shapes of the composite transducer.

lationship between the effective electro-mechanical coupling coefficient and the geometrical dimensions of the composite transducers for the first and second radial vibrational modes can be obtained as shown in Figure 9.

From Figure 9, it can be seen that when the thickness ratio τ is increased, the effective electro-mechanical coupling coefficient is accordingly increased. The reason for this phenomenon is that when the thickness ratio τ is increased, the proportion of the piezoelectric material in the transducer is increased; therefore, the effective electro-mechanical coupling coefficient is accordingly increased. On the other hand, it can also be seen that the effect of the

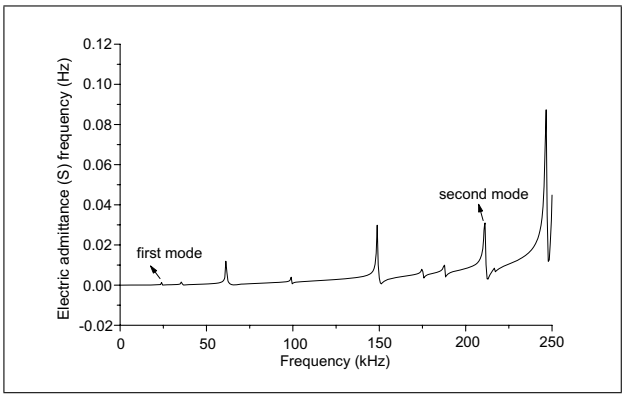


Figure 12. Numerically simulated electrical admittance response of the composite transducer.

geometrical dimension on the effective electro-mechanical coupling coefficient for the second radial mode is larger than that for the first radial vibrational mode; and the effective electro-mechanical coupling coefficient for the second radial vibration is larger than that for the first radial vibration of the radially polarized composite transducer. This conclusion can be useful in the design of practical radial transducers. By optimizing the geometrical dimensions and the radial vibrational modes, radial composite transducers with large effective electro-mechanical coupling coefficient can be designed and used in some related applications.

4. Finite element method simulation and experiments

In order to verify the analytical theory developed in the above sections, some radially composite ultrasonic transducers of the radially polarized piezoelectric ring and the metal ring are designed and manufactured as shown in Figure 10. The materials for the metal ring and the piezoelectric ring are hard aluminum and PZT-4. The material parameters for hard aluminum are:

$\rho = 2700\,\mathrm{kg/m^3}$, $E = 7.15 \cdot 10^{10}\,\mathrm{N/m^2}$, $\nu = 0.34$.

The material parameters for the piezoelectric material are the same as those in the above section. The geometrical dimensions for the transducers are listed in Tables I and II.

First, the finite element method (ANSYS Program) is used to simulate the radial vibration of the radially composite ultrasonic transducers. The simulated vibrational modal shape patterns are shown in Figure 11. It can be seen that for the first radial vibrational mode, the radial vibrational displacements on the inner and the outer cylindrical surfaces are in phase; while for the second radial vibrational mode, the radial vibrational displacements on the inner and the outer cylindrical surfaces are in opposite phase. Figure 12 is the numerically simulated input electrical admittance response of the No.2 composite transducer.

Second, the electric admittance response of the transducers is measured by using an Agilent 4294A Precision Impedance Analyzer. The measured admittance-frequency curve for the No.2 transducer is illustrated in Figure 13. In

Table I. Theoretical and experimental resonance frequencies of two radially composite ultrasonic transducers of the radially polarized piezoelectric ring and the metal ring.

No.	a (mm)	b (mm)	c (mm)	L (mm)	f_t (Hz)	f_n (Hz)	f_m (Hz)	Δ_1 (%)	Δ_2 (%)
1	11	15	21	17	42745	42427	43776	2.36	3.08
2	21	26	31	34	24322	24063	25679	5.28	6.29

Table II. Theoretical and experimental anti-resonance frequencies of two radially composite ultrasonic transducers of the radially polarized piezoelectric ring and the metal ring.

No.	a (mm)	b (mm)	c (mm)	L (mm)	f_t (Hz)	f_n (Hz)	f_m (Hz)	Δ_1 (%)	Δ_2 (%)
1	11	15	21	17	44189	43618	44226	0.08	1.37
2	21	26	31	34	25259	24762	25981	2.78	4.69

Figures 12 and 13, the admittance peaks correspond to the resonant vibrational modes of the composite transducers. It can be seen from Figures 12 and 13 that the positions for resonance peaks from the numerical method and the experiment are basically in agreement with each other. However, the admittance magnitudes of the numerical and experimental results are different. The reason may be that in the numerical simulation, the mechanical loss factor used is different from the real value of the materials, and this will definitely cause the difference.

For comparison, the analytical electric impedance response of the No.2 transducer is calculated according to equation (67) as shown in Figure 14. In the figure, the two impedance peaks respond to the first and second radial vibrational modes of the transducer. From Figures 12, 13 and 14, it can be seen that the analytical impedance response curve (Figure 14) is quite different from the numerically simulated and experimental results as shown in Figures 12 and 13. It is obvious that the analytical impedance response curve Figure 14 is simple; there are only two impedance peaks in a wide frequency bandwidth, which correspond to the first and second radial vibrational modes. The reason for this result is that in the analytical analysis of the composite transducer, the thin ring assumption is used and only radial vibration of the transducer is considered, therefore, other vibrational modes are not considered and there is no coupling between different vibrational modes. On the contrary, Figures 12 and 13 are the numerical simulated and experimental results for a practical transducer; its geometrical dimensions do not fully satisfy the condition of an ideal thin ring which is required in the theoretical analysis. In this case, apart from the radial vibration mode, other vibrational modes, such as the thickness vibration and the coupling vibration between the radial vibration and thickness vibration, can be produced, and therefore, the impedance or admittance response of the transducer becomes quite complicated, and more resonance peaks are produced.

The measured resonance and anti-resonance frequencies are listed in Table I and Table II. For comparison, the analytical results from the frequency equation and the numerically simulated results by using the ANASYS program are also given. In the table, f_t, f_n and f_m are

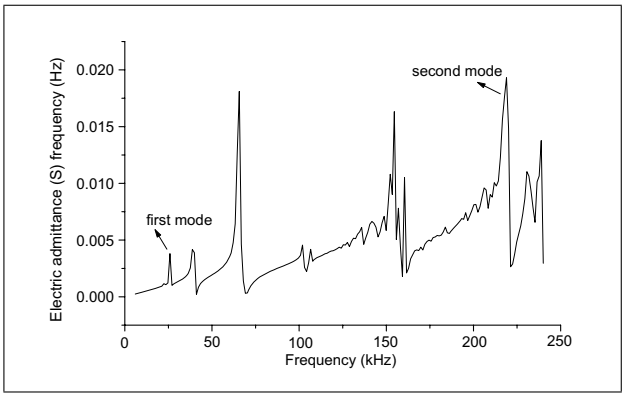


Figure 13. Experimental electrical admittance response of the composite transducer.

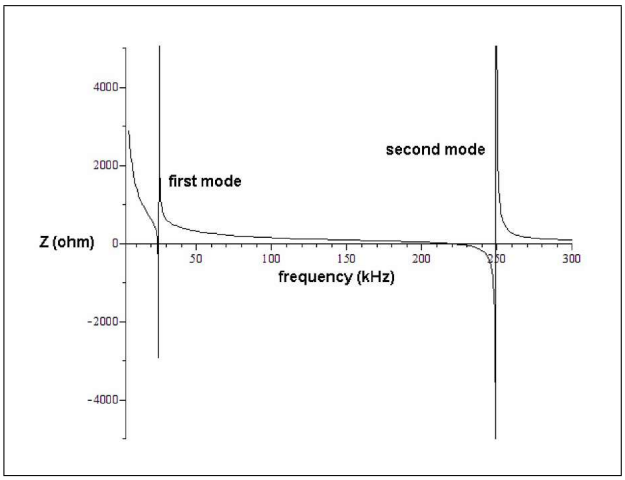


Figure 14. Analytical electrical impedance response of the composite transducer.

the analytical, numerical and experimental resonance/anti-resonance frequencies of the composite transducer, $\Delta_1 = |f_t - f_m|/f_m$, $\Delta_2 = |f_n - f_m|/f_m$,. It can be seen that they are in good agreement with each other.

As for the frequency error, the following factors should be considered. First, the standard material parameters are used in the theoretical calculation and simulation, they are more or less different from the real values of the materials

used. Second, in the assembly of the composite transducer, the method of heat expansion and cold contraction is used. Since the radial stress is difficult to control, the frequency error may be caused by the radial stress in the composite transducer. Third, the analytical theory used is based on the plane stress assumption, it requires that the height of the transducer should be much less than its radial dimension. However, for the real transducers, this condition is not completely satisfied. This is especially true for the No.2 transducer whose height is comparatively large, and the frequency error is therefore large compared with the No.1 transducer.

5. Conclusions

The radially composite cylindrical ultrasonic transducer of the radially polarized piezoelectric ceramic ring and the metal ring is studied. The exact solution for the radial vibration of a radially polarized piezoelectric ceramic thin ring with arbitrary wall thickness is given. The six-port electro-mechanical equivalent circuit of the composite transducer is obtained and the resonance/anti-resonance frequency equations are given. To sum up the above analysis, the following conclusions can be drawn.

1. The six-port electro-mechanical equivalent circuit for the radial vibration of a radially polarized piezoelectric ring is not symmetrical on the inner and the outer surfaces. It is more complicated and different from the traditional electro-mechanical equivalent circuits of the piezoelectric ring with different polarizations and vibrational modes, such as the thickness vibration and radial vibration of a piezoelectric ceramic ring with thickness polarization.
2. When the total radial thickness of the composite transducer is kept unchanged, the resonance/anti-resonance frequency of the transducer is decreased when the radial thickness of the piezoelectric ring is increased.
3. The effective electro-mechanical coupling coefficient of the second radial vibrational mode is larger than that of the first radial vibrational mode. It is expected that by choosing the geometrical dimensions and the vibrational orders of the transducer, optimization design for the radially composite transducer can be realized.
4. The analytical, numerical and experimental resonance/anti-resonance frequencies are in good agreement with each other.

Acknowledgement

The authors wish to acknowledge the National Natural Science Foundation of China (10974127, 10974128 and 11174192) and the Research Funds for the Doctoral Program of Higher Education of China (20110202110010) for their financial support.

References

[1] L. Parrini: New technology for the design of advanced ultrasonic transducers for high-power applications. Ultrasonics **41** (2003) 261–269.

[2] D. Chacon, G. Rodrıguez-Corral, L. Gaete-Garreton, E. Riera-Franco de Sarabia, J. A. Gallego-Juarez: A procedure for the efficient selection of piezoelectric ceramics constituting high-power ultrasonic transducers. Ultrasonics **44** (2006) e517–e521.

[3] E. Heikkola, K. Miettinen, P. Nieminen: Multiobjective optimization of an ultrasonic transducer using NIMBUS. Ultrasonics **44** (2006) 368–380.

[4] A. Iula, F. Vazquez, P. M., J. A. Gallego: Finite element three-dimensional analysis of the vibrational behaviourof the Langevin-type transducer. Ultrasonics **40** (2002) 513–517.

[5] A. Iula, R. Carotenuto, N. Lamberti, M. Pappalardo: An approximated 3-D model of the Langevin transducer and its experimental validation. Journal of the Acoustical Society of America **111** (2002) 2675–2680.

[6] P. S. L., A. S. Peshkovsky: Matching a transducer to water at cavitation: Acoustic horn design principles. Ultrasonics Sonochemistry **14** (2007) 314–322.

[7] O. Dahlem, J. Reisse, V. Halloin: The radially vibrating horn: A scaling-up possibility for sonochemical reactions. Chemical Engineering Science **54** (1999) 2829–2838.

[8] O. V. Abramov: High-intensity ultrasonics: theory and industrial applications. Gorden and Breach Science Publishers, Amsterdam, The Netherlands, 1998. 416-445.

[9] Walter et al.: Ultrasonic transducer [P]. United States: 5200666, 1993.

[10] S. Lin: Study on a new type of radial composite piezoelectric ultrasonic transducers in radial vibration. IEEE Transactions on Ultrasonics, Ferroelectrics, and Frequency Control **53** (2006) 1671–1678.

[11] S. Lin: Study on the radial composite piezoelectric ceramic transducer in radial vibration. Ultrasonics **46** (2007) 51–59.

[12] S. Lin: Electro-mechanical equivalent circuit of a piezoelectric ceramic thin circular ring in radial vibration. Sensors and Actuators A **134** (2007) 505–512.

[13] N. T. Adelman, Y. Stavsky, E. Segal: Axisymmetric vibrations of radially polarized piezoelectric ceramic cylinders. Journal of Sound and Vibration **38** (1975) 245–254.

[14] A. N. T., Y. Stavsky: Vibrations of radially polarized composite piezoceramic cylinders and disks. Journal of Sound and Vibration **43** (1975) 37–44.

[15] E. D. D.: Three-port parameters and equivalent circuit of radially polarized piezoelectric ceramic cylinders of finite length. J. Acoust. Soc. Am. **99** (1996) 2908–2912.

[16] J. O. Kim, H. K. K., H. G. Jeong: Radial vibration characteristics of piezoelectric cylindrical transducers. Journal of Sound and Vibration **276** (2004) 1135–1144.

[17] S. Liu, S. Lin: The analysis of the electro-mechanical model of the cylindrical radial composite piezoelectric ceramic transducer. Sensors and Actuators A: Physical **155** (2009) 175–180.

[18] S. Lin, S. Wang: Radially composite piezoelectric ceramic tubular transducer in radial vibration. IEEE Transactions on Ultrasonics, Ferroelectrics and Frequency Control **58** (2011) 2492–2498.

[19] A. Iula, N. Lamberti, R. Carotenuto, M. Pappalardo: Analysis of the radial symmetrical modes of thin piezoceramic rings. IEEE Transaction on Ultrasonics, Ferroelectrics and Frequency Control **46** (1999) 1047–1049.

[20] A. Iula, N. Lamberti, M. Pappalardo: A model for the theoretical characterization of thin piezoceramic rings. IEEE Trans. on Ultrasonic, Ferroelectric and Frequency Control **43** (1996) 370–375.

[21] S. Lin: Radial vibration and equivalent circuit of thin elastic circular rings (in Chinese). Acta Acustica **28** (2003) 102–106.

[22] C. H. Sherman, J. L. Butler: Transducers and arrays for underwater sound. Springer Science + Business Media, LLC, New York, 2007. 31-42.

[23] W. P. Mason: Physical acoustics, principles and methods. Volume 1, Part A. Academic Press, New York and London, 1964.

[24] O. E. Mattiat: Ultrasonic transducer materials. Plenum Press, New York and London, 1971.